OPEN ACCESS
IOP Publishing
Semiconductor Science and Technology
Semicond. Sci. Technol. **34** (2019) 035030 (6pp)
https://doi.org/10.1088/1361-6641/ab0518

Impact of iron on the room temperature luminescence efficiency of oxygen-containing precipitates in silicon

Karsten Bothe[1], **Sandra Herlufsen**[1] **and John D Murphy**[2,3]

[1] Institut für Solarenergieforschung Hameln/Emmerthal, Am Ohrberg 1, D-31860 Emmerthal, Germany
[2] School of Engineering, University of Warwick, Coventry, CV4 7AL, United Kingdom

E-mail: k.bothe@isfh.de and john.d.murphy@warwick.ac.uk

Received 17 July 2018, revised 23 January 2019
Accepted for publication 7 February 2019
Published 25 February 2019

Abstract

Oxygen precipitation in silicon has been associated with a weak room temperature sub-bandgap luminescence emission at around 1600 nm. We show that the additional presence of iron impurities enhances this emission by an order of magnitude and results in a red shift of the peak luminescence by approximately 45 nm. We not only observe an increase in the luminescence emission with iron contamination level but also with the density and size of the oxide precipitates. Moreover, we provide evidence that the sub-bandgap luminescence emission increases proportionally with the concentration of iron segregated to oxide precipitates after high temperature (>700 °C) annealing and thus allows evaluation of the gettering efficiency of oxygen-containing precipitates. Annealing of iron-contaminated samples at low temperatures (550 °C) results in a considerable reduction in the interstitial iron concentration without changing the sub-bandgap luminescence, indicating that the sink to which iron diffuses depends upon temperature.

Keywords: silicon, luminescence, photovoltaics, oxygen, gettering

(Some figures may appear in colour only in the online journal)

1. Introduction

Iron is known to be one of the most troublesome contaminants in silicon due to its capability to form minority carrier lifetime reducing defects [1, 2]. Complete elimination of iron from silicon device manufacturing is challenging. As iron is a very common element in nature, it is found in lower purity silicon feedstock and can enter silicon during crystal growth and subsequent device processing. Consequently, methods have been developed to remove iron from active device regions. In microelectronics, internal gettering by oxygen-containing precipitates is used to form defect-free near-surface regions for device manufacturing [3]. In solar cells—where the active device region is the whole bulk—this approach is counterproductive, since oxygen-containing precipitates [4–7] and, to an even greater extent metal-decorated oxygen-containing precipitates [6, 8, 9], are efficient recombination centres. Consequently, an extensive understanding of the interaction of oxide precipitates with metal impurities is of utmost relevance to microelectronics and photovoltaics.

Even though this topic has been studied for many decades not all physical aspects of the interaction between oxygen-containing precipitates and mobile metal contaminants are completely understood. In our previous work, we showed that strained oxide precipitates give rise to a broad room temperature luminescence peak centred at ~1600 nm increasing in intensity with the density of strained precipitates [10]. Such an emission has also been associated with oxide precipitates previously [11–16]. We also found that

[3] Author to whom any correspondence should be addressed

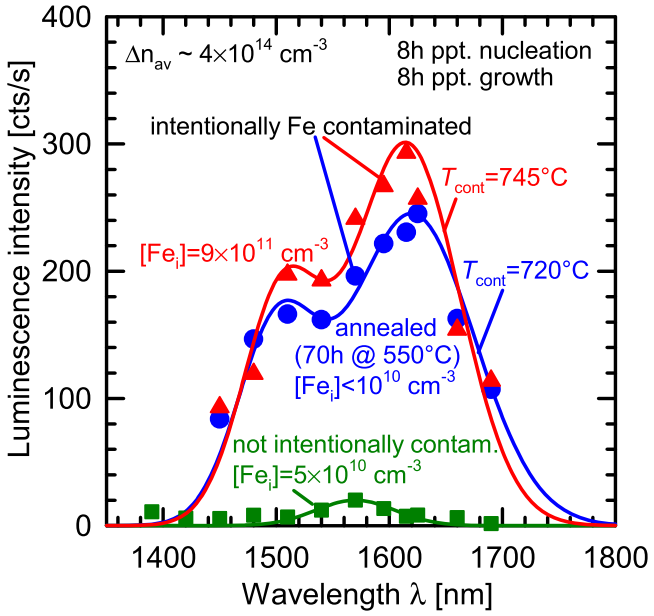

Figure 1. Spectrally resolved sub-bandgap PL measured in Cz–Si with an oxide precipitate density of $2.4 \pm 1 \times 10^9\,\mathrm{cm}^{-3}$. Iron contamination results in a significant increase in PL and a shift to longer wavelength by ~45 nm. A prolonged 550 °C anneal neither effects the spectral distribution nor the intensity of the luminescence to a nominal extend. The smaller peak intensity for the annealed sample is a consequence of the slightly lower contamination temperature.

dislocations and stacking faults around the oxide precipitates suppress this luminescence by introducing competitive non-radiative recombination centres [10]. By studying the impact of impurity decoration of oxide precipitates on the minority carrier lifetime, we found a clear relationship between the recombination rate and the concentration of iron segregated to the precipitates [6, 8]. Moreover we extracted the same set of recombination parameters for samples intentionally contaminated [6, 8, 9], and not intentionally contaminated by iron [5] suggesting that impurities are responsible for at least some of the recombination activity of oxygen-containing precipitates and that only very small quantities are required for substantial detrimental effects. In this work, we investigate the impact of iron contamination on the room temperature luminescence emission of *p*-type Czochralski silicon (Cz–Si) containing oxide precipitates of different sizes.

2. Experimental methods

Samples were cut from ~670 μm thick high-purity Cz–Si wafers with a diameter of 150 mm. The samples are boron doped with a concentration of $(1.3 \pm 0.2) \times 10^{15}\,\mathrm{cm}^{-3}$ and have an initial oxygen concentration (DIN50438/I) of $(7.7 \pm 0.2) \times 10^{17}\,\mathrm{cm}^{-3}$. The carbon content was below the FTIR detection limit of $5 \times 10^{15}\,\mathrm{cm}^{-3}$. Wafers were subjected to a four-stage precipitation treatment as described in [4] to create different densities and sizes of oxide precipitates. The treatment yielded a matrix of samples with widely different properties, as published in [10]. In the current paper we consider samples which have undergone an 8 h nucleation treatment and growth treatments of 0.5 h (blue), 8 h (green) and 16 h (red), respectively. The properties of the precipitates in these samples have been previously characterised by chemical etching and transmission electron microscopy (TEM), with results presented by other authors in [17, 18]. The precipitates in our 0.5 h growth samples were unobservable by TEM, and optical microscopy of etched samples gave a density of around $8 \times 10^7\,\mathrm{cm}^{-3}$. Our samples with the 8 h growth treatment were found to be single platelet precipitates, with particles found in TEM having a typical diameter of 50–60 nm, with some larger particles of diameter up to 120 nm observed. Optical microscopy of the 8 h growth samples revealed small lens-like pits on the cleaved surface with a density of $7 \times 10^8\,\mathrm{cm}^{-3}$, and the density from TEM was consistent with this. For the 16 h growth samples, optical microscopy revealed a density of around a density of $1 \times 10^9\,\mathrm{cm}^{-3}$ with lens-like etch pits larger than in the 8 h growth case with evidence for stacking faults around the precipitates. TEM on the 16 h growth samples revealed both linear precipitate-dislocation conglomerates and mixed linear/global precipitate-dislocation conglomerates. The mixed precipitate-dislocation conglomerates contain several platelet precipitates, large dislocation loops and some small defects that may be secondary precipitates. The platelet diameter is typically 180–200 nm while the overall size of the conglomerate is 3–3.5 μm. As published in [10], all samples' PL spectra show the characteristic *band-to-band* emission at 1100–1350 nm, as well as an additional broad *sub-bandgap* emission between 1400 and 1700 nm varying with the precipitation treatments.

Great care was taken to avoid impurity contamination during the processing to create the oxide precipitates. The bulk iron concentration of these samples before any intentional contamination was measured by photodissociation of iron boron pairs [19, 20] to be below $4 \times 10^{11}\,\mathrm{cm}^{-3}$. The method and calculation we use to determine the interstitial iron concentration is described in detail in our previous publication [4]. The method involves subjecting the sample to intense flashes of illumination at room temperature to dissociate the FeB pairs. On the assumption that the lifetime changes are only due to FeB pair dissociation then the change in lifetime is related to concentration of interstitial iron by Shockley–Read–Hall statistics as detailed in our previous paper [4]. To study the impact of iron, *intentional* iron contamination was achieved for specific samples by rubbing the back-sides of $(5 \times 5)\,\mathrm{cm}^2$ samples with iron pieces (99.95% purity from Testbourne Limited, UK). Samples were then annealed in air in a pre-heated furnace at temperatures up to 775 °C for times chosen to ensure complete iron diffusion through the sample. Cooling was rapid, with the samples removed from the furnace at temperature and placed on a heat sink. It is estimated that rapidly cooled samples were cooled to below ~100 °C in <10 s to minimise iron precipitation. In oxide precipitate-free samples, an iron solubility of $[\mathrm{Fe_i}]_{\max} = 1.3 \times 10^{21} \exp\left(-\frac{1.8\,\mathrm{eV}}{kT}\right)\,\mathrm{cm}^{-3}$ was found, where T is the absolute contamination temperature [21, 22]. All

samples were subjected to an HF dip, an RCA clean, and SiN_x surface passivation using remote plasma enhanced chemical vapour deposition. The passivation scheme used has previously been shown to give a surface recombination velocity below 10 cm s^{-1} [23]. Passivation involved the samples being at 400 °C for ~10 min, and although SiN_x films have been found to getter iron impurities from the bulk [24] only minimal gettering is expected for this temperature and time.

Photoluminescence (PL) emission is detected using the set-up described in [10, 25] which uses an indium gallium arsenide (InGaAs) complementary metal-oxide semiconductor focal plane array as detector. Broadband sub-bandgap luminescence is measured with an optical 1450 nm long pass filter. For all wavelength-dependent measurements, we use optical band-pass filters with central wavelengths ranging from 1115 to 1690 nm and having a maximum bandwidth of 25–30 nm. All values reported are area-averaged over ~(4 × 4) cm^2. For carrier excitation, we use a high power laser diode with a central wavelength of 805 nm connected to a micro lens beam homogeniser resulting in a min-max intensity variation of 10% across the sample area.

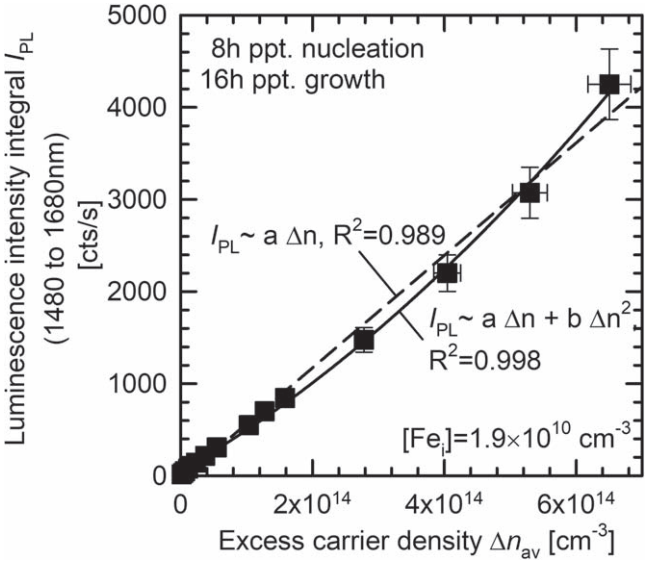

Figure 2. Typical relationship between the broadband room temperature sub-bandgap luminescence and the excess carrier density generated by optical excitation. Linear and quadratic fits are shown, with a better fit demonstrated in the quadratic case.

3. Results and discussion

Figure 1 shows the sub-bandgap PL signal at an excess carrier density of $\Delta n = 4 \times 10^{14}$ cm^{-3} as a function of wavelength for three samples with the same oxide precipitate density of $(2.4 \pm 1) \times 10^9$ cm^{-3} (arising from 8 h nucleation and 8 h growth times) subjected to different processes. One sample had not been subjected to a contamination anneal (green squares), and the two other samples have been contaminated with iron with one (blue circles) also subjected to an extended anneal (70 h) at a lower temperature (550 °C). The most significant result is that sub-bandgap luminescence increases by approximately one order of magnitude after the intentional iron contamination. The PL increase is accompanied by a peak shift from 1570 to 1615 nm and the appearance of a less pronounced side peak at 1510 nm. By photodissociation of FeB pairs [19], we determine an interstitial iron concentration of 4.6 × 10^{10} cm^{-3} for the sample which had not been intentionally contaminated, and respective interstitial iron concentrations of 8.7 × 10^{11} cm^{-3} (red triangles) and $<10^{10}$ cm^{-3} (blue circles) for the samples contaminated with and without the low temperature subsequent anneal. The fact that the luminescence is at a similarly high level in both the red and blue datasets in figure 1 despite the large different in interstitial iron concentration shows that the interstitial iron itself is not responsible for the increased sub-bandgap luminescence. It seems likely that the iron impurities at the oxide precipitates and surrounding defects are responsible for the enhanced luminescence and it is noted that the interstitial iron measurement technique is not sensitive to the detection of such iron.

In [10], we proposed a possible model for the sub-bandgap PL in terms of defect energy levels relating to oxide precipitates and surrounding defects in samples not intentionally contaminated with impurities. As we have since shown the same energy levels exist in iron-contaminated samples [6, 8, 9], the sub-bandgap PL emission shown in figure 1 for contaminated samples is consistent with the same model proposed previously. Small shifts in sub-bandgap PL observed are likely due to small changes in the local structure of the iron impurities at the precipitates, as well as the precipitates themselves, but it is not possible to determine such differences accurately in a room temperature PL study.

For a more detailed study on the interaction of oxide precipitates and iron, we first measure the PL emission as a function of the optically excited excess carrier density (Δn). The corresponding excess carrier density is determined from the photoconductance of the sample measured simultaneously using a Sinton Instruments WCT-120 system integrated into the PL setup [26, 27]. As shown exemplarily in figure 2, in oxide precipitate containing samples the sub-bandgap PL increases strongly with the excess carrier density. Consequently, we have to ensure constant excess carrier conditions if we want to compare the sub-bandgap luminescence intensity. As the recombination strength of competing recombination channels varies from sample to sample (carrier lifetimes vary by approximately two orders of magnitude), the excitation power was tuned for each sample. For samples with a larger number of recombination channels, the laser power was increased, while for samples with lower competing recombination activity the laser power was reduced. Thus, for all measurements presented in this paper, we adjust the laser power, and hence the photogeneration rate, to obtain the same average excess carrier density of $\Delta n_{av} \approx 10^{14}$$cm^{-3}$ as measured with the integrated photoconductance measurement stage. This required photon fluxes in the range 1.8×10^{16}–3.4×10^{18} cm^{-2} s^{-1}. Furthermore, the specific charge carrier density was carefully chosen to prevent changes in the free (unprecipitated) iron (Fe_i) concentration from affecting the measurement results. Such changes may occur

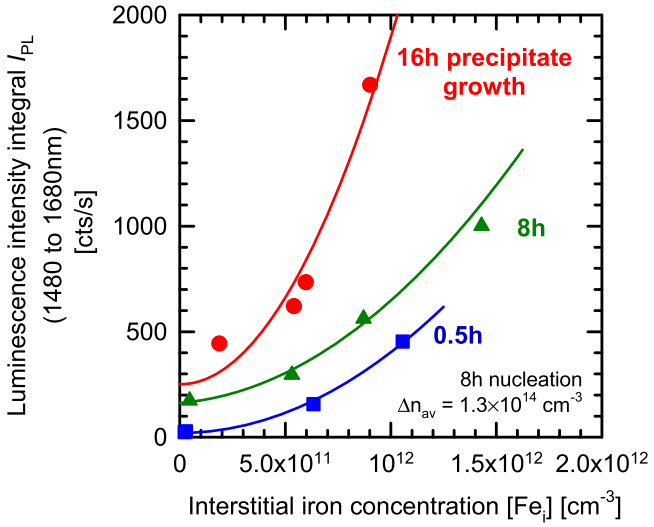

Figure 3. Broadband sub-bandgap luminescence as a function of the interstitial iron concentration for samples with different oxide precipitate growth times and hence precipitate sizes.

since iron-boron pairs (FeB) tend to dissociate under illumination. However, at an excess carrier density of $\Delta n_{av} \approx 10^{14}$ cm^{-3} the lifetime versus excess carrier density curves related to recombination at FeB and Fe_i intersect [28] and consequently the carrier lifetime does not depend on the percentage of FeB pairs dissociated.

In general, the variation of PL signal with excess electron density is related to the number of carriers involved in the signal generation. If only an electron is required to generate the PL signal then a linear dependence is expected, whereas if both an electron and hole are required a quadratic dependence will result (as in the case of band-to-band emission [29]). Within the measurement uncertainties, the dependence of sub-bandgap PL signal on excess carrier density shown in figure 2 can be described by either a linear or quadratic equation. However, the coefficient of determination is closer to 1 for the quadratic fit suggesting a quadratic dependence of the PL signal on Δn. This suggests that the origin of the sub-bandgap PL could be due to a bimolecular process involving electrons and holes. This would be consistent with our previously proposed model [10] involving two defect bands within the bandgap, with one having a relatively large hole capture cross-section and the other having a relatively large electron capture cross-section.

The results in figure 3 show the application of such measurements to samples subjected to the same precipitate nucleation treatment but different growth times. The relationship between growth time and precipitate size is complicated by the morphological transformation which is known to occur for oxide precipitate growth in silicon [17, 30]. Precipitates are initially unstrained (and do not give rise to a sub bandgap PL signal [10]) and with increasing growth time gradually convert into strained precipitates which give rise to sub bandgap PL and these then grow in size with further annealing. Our previous work has shown the density for 8 h nucleation to have reach its maximum value after 8 h of growth time [4]. Thus the key difference between the 8 h growth (green) and 16 h growth (red) data in figure 3 is that the precipitates are larger in the latter. For each growth time the broadband sub-bandgap luminescence also increases with interstitial iron concentration, but, as already shown in figure 1, *interstitial* iron is not the cause for the increased luminescence. The origin of the increased luminescence is the increased concentration of iron in the vicinity of the oxide precipitates.

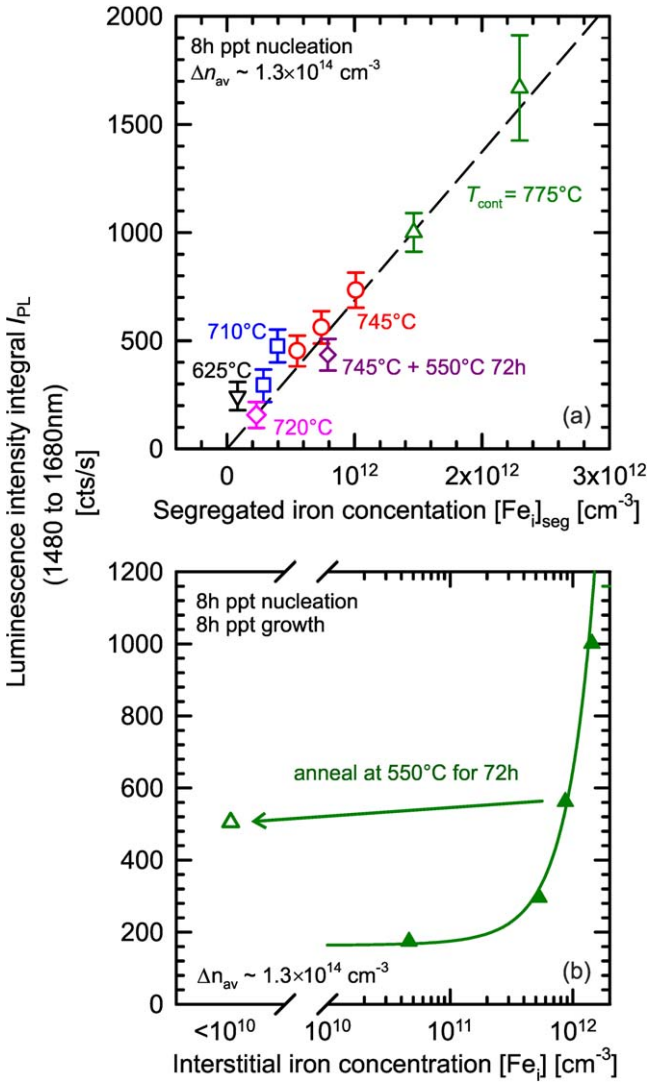

Figure 4. (a) Broadband sub-bandgap luminescence as a function of the iron concentration segregated to oxygen precipitates. (b) Impact of prolonged 550 °C anneal on broadband sub-bandgap luminescence and interstitial iron concentration.

In figure 4(a) we show the broadband sub-bandgap PL as a function of the amount of iron segregated to oxygen precipitates. The segregated iron concentration $[Fe_i]_{seg}$ is calculated from the iron solubility limit of Murphy and Falster [21, 22] and the free interstitial iron concentration according to $[Fe_i]_{seg} = [Fe_i]_{max} - [Fe_i]$, where $[Fe_i]$ is the interstitial iron concentration measured in a given sample. Figure 4(a) shows a nearly proportional increase in the sub-bandgap luminescence with the segregated iron concentration. These results suggest that the sub-bandgap PL mechanism is

enhanced by the simultaneous presence of iron and oxygen-containing precipitates. This is similar to our previous lifetime studies in which we extracted the same set of recombination parameters for samples intentionally contaminated [8] and not intentionally contaminated with iron [5], with only the state density required as a fitting parameter. This explanation is consistent with the data shown in figure 3 as larger precipitates are able to capture larger concentrations of iron impurities.

Figure 4(b) shows the broadband sub-bandgap luminescence signal as a function of the interstitial iron concentration defined by varying the contamination temperature for a fixed density and size of oxide precipitates. One sample was annealed for 72 h at a temperature of 550 °C as used for internal gettering in multi-crystalline silicon [31, 32]. This prolonged annealing step results in considerable reduction in the *free* interstitial iron concentration to below the detection limit of the photodissociation approach of approximately $10^{10}\,\mathrm{cm}^{-3}$. Surprisingly, as also shown in figure 1, the sub-bandgap luminescence intensity is not affected. From this we conclude that during the lower temperature annealing step, iron atoms may segregate to different sites, form iron precipitates in the bulk or exist in a different state in the vicinity of the oxide precipitates than at higher temperatures. Alternatively, given the long duration of the 550 °C anneal (72 h), it is kinetically possible for the interstitial iron to have been gettered preferentially to the free surfaces of the sample [22]. One difference of this prolonged annealing step compared to the iron contamination approach is the temperature.

4. Conclusions

In summary, we have studied room temperature sub-bandgap PL in single crystal silicon processed thermally to contain oxide precipitates. We find the well-known PL signal at around 1600 nm to be strongly enhanced by contamination of the samples with iron. Moreover, our investigations revealed a correlation between the PL emission intensity and the concentration of iron segregated to oxide precipitates. This provides a potential method to quantify impurity gettering by oxide precipitates in silicon at temperatures above 600 °C. Although the enhancement of the emission is only by approximately one order of magnitude, it is well controlled and occurs at room temperature, and thus it could find a future use as an optical emitter in silicon-based photonic devices for optoelectronic applications.

Acknowledgments

We are very grateful to Dr Robert Falster for providing the silicon samples containing the oxide precipitates. KB and SH thank Mirjam Gutbrod for countless PL measurements and her patience with our endless wishes for new experiments. JDM acknowledges the financial support of the EPSRC SuperSilicon PV project (EP/M024911/1). Data published in this article can be freely downloaded from https://wrap.warwick.ac.uk/113535/.

ORCID iDs

Karsten Bothe https://orcid.org/0000-0001-9369-2429
John D Murphy https://orcid.org/0000-0003-0993-5972

References

[1] Myers S M, Seibt M and Schröter W 2000 Mechanisms of transition-metal gettering in silicon *J. Appl. Phys.* **88** 3795
[2] Istratov A A, Hieslmair H and Weber E R 2000 Iron contamination in silicon technology *Appl. Phys.* A **70** 489
[3] Gilles D, Weber E R and Hahn S 1990 Mechanism of internal gettering of interstitial impurities in Czochralski-grown silicon *Phys. Rev. Lett.* **64** 196
[4] Murphy J D, Bothe K, Olmo M, Voronkov V V and Falster R J 2011 The effect of oxide precipitates on minority carrier lifetime in p-type silicon *J. Appl. Phys.* **110** 053713
[5] Murphy J D, Bothe K, Krain R, Voronkov V V and Falster R J 2012 Parameterisation of injection-dependent lifetime measurements in semiconductors in terms of Shockley–Read–Hall statistics: an application to oxide precipitates in silicon *J. Appl. Phys.* **111** 113709
[6] Murphy J D, McGuire R E, Bothe K, Voronkov V V and Falster R J 2014 Minority carrier lifetime in silicon photovoltaics: the effect of oxygen precipitation *Sol. Energy Mater. Sol. Cells* **120** 402
[7] Le Donne A, Binetti S, Folegatti V and Coletti G 2016 On the nature of striations in n-type silicon solar cells *Appl. Phys. Lett.* **109** 033907
[8] Murphy J D, Bothe K, Voronkov V V and Falster R J 2013 On the mechanism of recombination at oxide precipitates in silicon *Appl. Phys. Lett.* **102** 042105
[9] Murphy J D, McGuire R E, Bothe K, Voronkov V V and Falster R J 2014 Competitive gettering of iron in silicon photovoltaics: oxide precipitates versus phosphorus diffusion *J. Appl. Phys.* **116** 053514
[10] Bothe K, Falster R J and Murphy J D 2012 Room temperature sub-bandgap photoluminescence from silicon containing oxide precipitates *Appl. Phys. Lett.* **101** 032107
[11] Kitagawara Y, Hoshi R and Takenaka T 1992 Evaluation of oxygen precipitated silicon crystals by deep-level photoluminescence at room temperature and its mapping *J. Electrochem. Soc.* **139** 2277
[12] Tajima M, Tokita M and Warashina M 1995 Photoluminescence due to oxygen precipitates distinguished from the D lines in annealed Si *Mater. Sci. Forum* **196-201** 1749
[13] Binetti S, Pizzini S, Leoni E, Somaschini R, Castaldini A and Cavallini A 2002 Optical properties of oxygen precipitates and dislocations in silicon *J. Appl. Phys.* **92** 2437
[14] Pizzini S, Binetti S, Leoni E, Le Donne A, Acciarri M and Castaldini A 2002 Radiative recombination processes of thermal donors in silicon *Mater. Res. Soc. Symp. Proc.* **692** H6.30.1
[15] Tajima M, Ikebe M, Ohshita Y and Ogura A 2010 Photoluminescence analysis of iron contamination effect in multicrystalline silicon wafers for solar cells *J. Electron. Mater.* **39** 747
[16] Tajima M, Ishikawa Y, Kiuchi H and Ogura A 2018 Origin of room-temperature photoluminescence around C-line in

electron-irradiated Si and its applicability for quantification of carbon *Appl. Phys. Express* **11** 041301
[17] Falster R, Voronkov V V, Resnik V Y and Milvidskii M G 2004 Thresholds for effective internal gettering in silicon wafers *Proc. Electrochemical Society, High Purity Silicon VIII* vol 200405, p 188
[18] Falster R J, Voronkov V V, Resnick V Y and Mil'vidskii M G 2005 Morphological transformation of oxide particles and thresholds for effective gettering in silicon *Solid State Phenom.* **108–109** 97
[19] Zoth G and Bergholz W 1990 A fast, preparation-free method to detect iron in silicon *J. Appl. Phys.* **67** 6764
[20] Rein S and Glunz S W 2005 Electronic properties of interstitial iron and iron-boron pairs determined by means of advanced lifetime spectroscopy *J. Appl. Phys.* **98** 113711
[21] Murphy J D and Falster R J 2011 Contamination of silicon by iron at temperatures below 800 °C *Phys. Status Solidi Rapid Res. Lett.* **5** 370
[22] Murphy J D and Falster R J 2012 The relaxation behaviour of supersaturated iron in single-crystal silicon at 500 to 750 °C *J. Appl. Phys.* **112** 113506
[23] Lauinger T, Moschner J, Aberle A G and Hezel R 1998 Optimization and characterization of remote plasma-enhanced chemical vapor deposition silicon nitride for the passivation of p-type crystalline silicon surfaces *J. Vac. Sci. Technol.* A **16** 530
[24] Liu A Y, Sun C, Markevich V P, Peaker A R, Murphy J D and Macdonald D 2016 Gettering of interstitial iron in silicon by plasma-enhanced chemical vapour deposited silicon nitride films *J. Appl. Phys.* **120** 193103
[25] Hinken D, Schinke C, Herlufsen S, Schmidt A, Bothe K and Brendel R 2011 Experimental setup for camera-based measurements of electrically and optically stimulated luminescence of silicon solar cells and wafers *Rev. Sci. Instrum.* **82** 033706
[26] Sinton R A and Cuevas A 1996 Contactless determination of current–voltage characteristics and minority-carrier lifetimes in semiconductors from quasi-steady-state photoconductance data *Appl. Phys. Lett.* **69** 2510
[27] Herlufsen S, Schmidt J, Hinken D, Bothe K and Brendel R 2008 Photoconductance-calibrated photoluminescence lifetime imaging of crystalline silicon *Phys. Status Solidi Rapid Res. Lett.* **2** 245
[28] Birkholz J E, Bothe K, Macdonald D and Schmidt J 2005 Electronic properties of iron-boron pairs in crystalline silicon by temperature- and injection-level-dependent lifetime measurements *J. Appl. Phys.* **97** 103708
[29] Schlangenotto H, Maeder H and Gerlach W 1974 Temperature dependence of the radiative recombination coefficient in silicon *Phys. Status Solidi* A **21** 357
[30] Bergholz W, Binns M J, Booker G R, Hutchison J C, Kinder S H, Messoloras S, Newman R C, Stewart R J and Wilkes J G 1989 A study of oxygen precipitation in silicon using high-resolution transmission electron microscopy, small-angle neutron scattering and infrared absorption *Phil. Mag.* B **59** 499
[31] Krain R, Herlufsen S and Schmidt J 2008 Internal gettering of iron in multicrystalline silicon at low temperature *Appl. Phys. Lett.* **93** 152108
[32] Liu A Y and Macdonald D 2014 Precipitation of iron in multicrystalline silicon during annealing *J. Appl. Phys.* **115** 114901